# Semi-transparent Solar Cells: Strategies for Maximum Power Output in Cities

Vox Kalai Wong[a], Johnny Ka Wai Ho[a], Wallace W. H. Wong[b], Shu Kong So*[a]

[a] *Department of Physics and Institute of Advanced Materials, Hong Kong Baptist University, Hong Kong Special Administrative Region, China*

[b] *ARC Centre of Excellence in Exciton Science, School of Chemistry, The University of Melbourne, Parkville, Victoria 3010, Australia*

## Supplementary Information

### S1. Strategy-dependent absorptance $A_G^r(\lambda)$

The harvestable irradiance spectrum extracts a portion of a solar spectrum for the STPV absorber through an absorption profile. The absorptance $A_G^r(\lambda)$ depends on the spectral region $r$ ($r$ = UV, VIS, IR) and the absorption strategy $G$ (Fig. 1 (b)). The absorption strategy $G$ is a set containing the labels of absorption methods (neutral density (ND) and band selective (BS)) and absorption modes (UV, IR, and dual). The six strategies are {ND, UV}, {ND, IR}, {ND, UV, IR}, {BS, UV}, {BS, IR}, {BS, UV, IR}.

Table S2 contains the expressions of $A_G^r(\lambda)$ for the combinations of the three spectral regions $r$ and six strategies $G$. The UV and IR regions undergo complete absorption if strategy $G$ contains the region $r$ (e.g. $A_{\text{ND, UV}}^{\text{UV}}(\lambda) = A_{\text{BS, UV, IR}}^{\text{IR}}(\lambda) = 1$), and no absorption if not (e.g. $A_{\text{ND, UV}}^{\text{IR}}(\lambda) = A_{\text{BS, IR}}^{\text{UV}}(\lambda) = 0$). For $r$ = VIS, $A_G^{\text{VIS}}(\lambda)$ is parametrized by the wavelength-independent ND absorptance $A_G^{\text{VIS}} \in [0,1]$ when adopting the ND method and by the cutoff wavelength $\lambda_0 \in (400, 700]$ when adopting the BS method (Fig. S1). It can be summarized by Eq. (S1):

$$A_G^r\left(\lambda \in \left(\lambda_{\min}^r, \lambda_{\max}^r\right]\right) = \begin{cases} \mathbf{1}_G(r), & r = \text{UV, IR} \\ A_G^{\text{VIS}}, & r = \text{VIS, ND} \in G, \\ A_{\text{BS},i}^{\text{VIS}}(\lambda;\lambda_0), & r = \text{VIS, BS} \in G \end{cases} \tag{S1}$$

where $\mathbf{1}_G(r)$ is the indicator function (or characteristic function) of the set $G$. Note that $A_G^{\text{VIS}}(\lambda)$ modulates the absorber AVT. As the absorber AVT increases, the ND method lowers the VIS absorptance uniformly; $\lambda_0$ decreases for {BS, UV}, leaving the red-end VIS photons unabsorbed; $\lambda_0$ increases for {BS, IR}, leaving the violet-end photons unabsorbed; $\lambda_0$ shifts away from the centre in the VIS region for {BS, UV, IR}, absorbing only photons at the VIS ends (Fig. S1). Consequently, the absorption profile in the VIS region can be written as

$$A_{\text{BS},i}^{\text{VIS}}(\lambda;\lambda_0) = \begin{cases} 1-\theta(\lambda_0), & i = \text{UV} \\ \theta(\lambda_0), & i = \text{IR} \\ \delta_{2\left|\lambda_{\text{m}}^{\text{VIS}}-\lambda_0\right|}[\theta]\left(\lambda-\lambda_{\text{m}}^{\text{VIS}}\right), & i = \text{UV, IR} \end{cases}, \tag{S2}$$

where $\lambda_{\text{m}}^{\text{VIS}} = \left(\lambda_{\min}^{\text{VIS}} + \lambda_{\max}^{\text{VIS}}\right)/2$, $\theta(\lambda)$ is the Heaviside step function, and $\delta_{\Delta\lambda}[\theta](\lambda) = \theta(\lambda+\Delta\lambda) - \theta(\lambda-\Delta\lambda)$ is the central difference of the function $\theta$ with a spacing $\Delta\lambda$. In this study, $\lambda_{\min}^{\text{VIS}} = 400$ nm, $\lambda_{\max}^{\text{VIS}} = 700$ nm, and thus $\lambda_{\text{m}}^{\text{VIS}} = 550$ nm.

## S2. The Shockley–Queisser (SQ) Limit

The SQ-limited efficiency ($\eta_{SQ}$) is constrained by the ultimate efficiency ($\eta_u$), detailed-balance efficiency ($\eta_d$) and the fill factor (FF) loss ($\eta_{FF}$), i.e.

$$\eta_{SQ} = \eta_u \times \eta_d \times \eta_{FF}. \tag{S3}$$

The SQ device has a perfect absorber layer as the sole component that harnesses light, exhibiting complete absorption above the bandgap $E_g$ / eV and complete transmission otherwise. One incoming photon with energy higher than $E_g$ excites one and only one electron-hole (e-h) pair. Any e-h pair energy over $E_g$ undergoes thermal relaxation, resulting in a population of e-h pairs of the same energy $E_g$. Radiative recombination in the form of blackbody radiation is regarded as the only unavoidable recombination in this ideal device. In brief, the ultimate efficiency is defined as the ratio of the power intensity of all generated e-h pairs $P_{eh}$ to the solar irradiance $P_{in}$ / W m$^{-2}$, given by

$$\eta_u = \frac{P_{eh}}{P_{in}} = \frac{E_g \int_{E_g}^{\infty} \tilde{\Phi}_{S;G}(\epsilon) \cdot \frac{1}{\epsilon} \mathrm{d}\epsilon}{\int_{E_g}^{\infty} \Phi_S(\epsilon) \cdot \frac{1}{\epsilon} \mathrm{d}\epsilon}. \tag{S4}$$

$\Phi_S(\epsilon)$ and $\tilde{\Phi}_{S;G}(\epsilon)$ are the spectral solar irradiance and spectral harvestable irradiance in the energy domain (W m$^{-2}$ eV$^{-1}$). They can be interconverted with the wavelength domain (W m$^{-2}$ nm$^{-1}$) by

$$\Phi\left(\epsilon = \frac{hc}{\lambda}\right) = \Phi(\lambda) \cdot \frac{\lambda^2}{hc} \tag{S5}$$

where $h$ is the Planck's constant and $c$ is the speed of light.

Detailed balance considers the thermal equilibrium with steady rates of incoming and outgoing radiations. Radiative loss as blackbody radiation is modelled as the dark current, reducing the open-circuit voltage ($V_{oc}$). The detailed-balance efficiency is defined as the ratio of the potential energy at the open-circuit condition under detailed balance to the bandgap energy, i.e.

$$\eta_d = \frac{qV_{oc}^{SQ}}{E_g} = \frac{k_B T}{E_g} \ln\left(\frac{F_{eh}}{F_{0,rad}} + 1\right) \tag{S6}$$

where $V_{oc}^{SQ}$ is the SQ-limited $V_{oc}$ under detailed balance, $T$ is the temperature of the device under test, $q$ is the carrier charge, and $k_B$ is the Boltzmann's constant. $F_{eh}$ is the photon incident rate, given by

$$F_{eh} = \frac{P_{eh}}{E_g} = \int_{E_g}^{\infty} \tilde{\Phi}_{S;G}(\epsilon) \cdot \frac{1}{\epsilon} \mathrm{d}\epsilon, \tag{S7}$$

and $F_{0,rad}$ is the rate of emitted photon expressed in the form of blackbody radiation:

$$F_{0,rad} = \frac{4\pi}{h^3 c^2} \int_{E_g}^{\infty} \frac{\epsilon^2 \mathrm{d}\epsilon}{\exp\left(\epsilon / k_B T\right) - 1}. \tag{S8}$$

An SQ device assumes no finite shunt and series resistances. FF can then be written in the Green's empirical form[1]:

$$\eta_{FF} = 1 - \frac{1 + \ln\left(v_{oc}^{SQ} + 0.72\right)}{1 + v_{oc}^{SQ}} \tag{S9}$$

where $v_{oc}^{SQ} = qV_{oc}^{SQ}/k_BT = \eta_d E_g/k_BT$ is the normalized open-circuit voltage.

Table S1 Relative intensities $w_S^r$ in the UV, VIS, and IR regions for the Monthly Max. and Cloudy Average irradiance conditions, defined in Eq. (2). The values correspond to those in Fig. 3 (b).

| $r$ | $S$ = 0 (AM1.5G) | $S$ = Monthly Max. | $S$ = Cloudy Average |
|---|---|---|---|
| UV | 1 | 1.086 | 0.146 |
| VIS | 1 | 0.855 | 0.108 |
| IR | 1 | 0.779 | 0.079 |

Table S2 Expressions of $A_G^r(\lambda)$ in Eq. (S1) and Eq. (S2). $A_{ND,UV}^{VIS}$, $A_{ND,IR}^{VIS}$, $A_{ND,UV,IR}^{VIS}$, and $\lambda_0$ are input parameters that modulate the absorber AVT. Note $\lambda_{min}^{VIS} = 400$ nm, $\lambda_{max}^{VIS} = 700$ nm, and $\lambda_m^{VIS} = 550$ nm.

| | | Spectral region $r$ | | |
|---|---|---|---|---|
| | | UV ($280 \le \lambda < 400$) / nm | VIS ($400 \le \lambda < 700$) / nm | IR ($700 \le \lambda < 4000$) / nm |
| Strategy $G$ | {ND, UV} | 1 | $0 \le A_{ND,UV}^{VIS} \le 1$ | 0 |
| | {ND, IR} | 0 | $0 \le A_{ND,IR}^{VIS} \le 1$ | 1 |
| | {ND, UV, IR} | 1 | $0 \le A_{ND,UV,IR}^{VIS} \le 1$ | 1 |
| | {BS, UV} | 1 | $\begin{cases} 1, & 400\text{ nm} \le \lambda < \lambda_0 \\ 0, & \lambda_0 \le \lambda < 700\text{ nm} \end{cases}$ | 0 |
| | {BS, IR} | 0 | $\begin{cases} 0, & 400\text{ nm} \le \lambda < \lambda_0 \\ 1, & \lambda_0 \le \lambda < 700\text{ nm} \end{cases}$ | 1 |
| | {BS, UV, IR} | 1 | $\begin{cases} 0, & \lvert\lambda - 550\text{ nm}\rvert \le \lvert\lambda_0 - 550\text{ nm}\rvert \\ 1, & \text{otherwise} \end{cases}$ | 1 |

Table S3 Coefficients of the linear regression in the form $y = a + b \times$ absorber AVT with different absorption modes using the ND method, where $y$ is the maximum possible PCE (output power intensity). The $y$-intercept is fixed at the calculated Shockley–Queisser (SQ) limit at 0 % absorber AVT. $b$ is given in per absorber-AVT (%).

| | | {ND, UV} | | {ND, IR} | | {ND, UV, IR} | |
|---|---|---|---|---|---|---|---|
| | | PCE (%) | $P_{out}$ (W/m$^2$) | PCE (%) | $P_{out}$ (W/m$^2$) | PCE (%) | $P_{out}$ (W/m$^2$) |
| AM1.5G | Slope $b$ | -0.25774 | -257.833 | -0.14476 | -144.817 | -0.14976 | -149.817 |
| | $y$-intercept $a$ | 27.346 | 273.5566 | 31.784 | 317.957 | 33.081 | 330.9314 |
| Monthly Max. | Slope $b$ | -0.26633 | -220.011 | -0.15429 | -127.458 | -0.16101 | -133.014 |
| | $y$-intercept $a$ | 28.74 | 237.4191 | 31.471 | 259.9774 | 33.206 | 274.3149 |
| Cloudy Avg. | Slope $b$ | -0.28251 | -26.7236 | -0.17716 | -16.7579 | -0.18383 | -17.3893 |
| | $y$-intercept $a$ | 30.622 | 28.9662 | 30.281 | 28.64345 | 32.259 | 30.51426 |

Table S4 The peak light utilization efficiency (LUE) summarized over the irradiance conditions using the neutral density (ND) and band selective methods and the UV, IR and UV + IR absorption modes. The corresponding average visible transmittance (AVT) is stated in paratheses.

| | UV Mode | IR Mode | UV + IR Mode |
|---|---|---|---|
| Neutral Density (ND) | 7.2–8.2 % (50 % AVT) | 13–18 % (100 % AVT) | 14–19 % (100 % AVT) |
| Band Selective (BS) | 12–15 % (88 % AVT) | 16–20 % (94 % AVT) | 20–23 % (90 % AVT) |

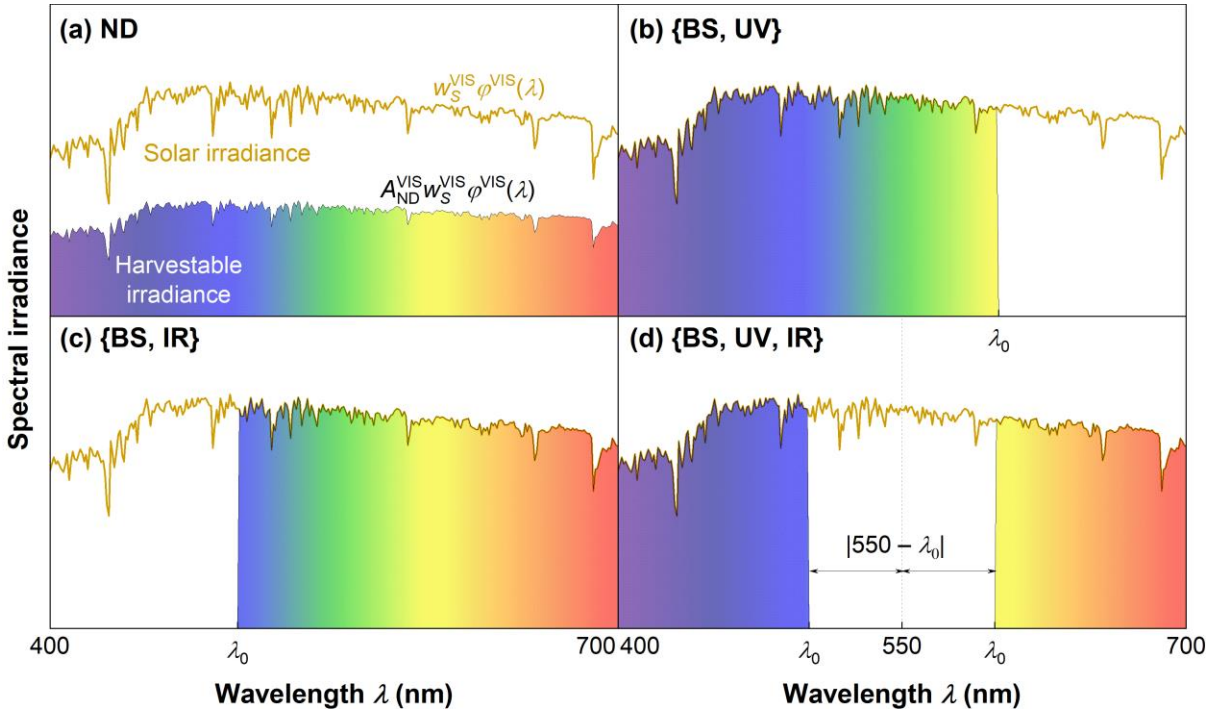


Fig. S1 Schematic illustration of absorption strategies parametrized in Eq. (S1) and Eq. (S2): (a) the ND method ({ND, UV}, {ND, IR}, and {ND, UV, IR}, (b) {BS, UV}, (c) {BS, IR}, and (d) {BS, UV, IR}. In (a), the harvestable irradiance spectrum scales down by a constant factor of $A_{\mathrm{ND}}^{\mathrm{VIS}}$. In (b–d), the harvestable irradiance spectrum is modulated by the cutoff wavelength $\lambda_0$. In (d), the cutoff wavelength can be specified by either end, as denoted in Eq. (S2) and Table S2.

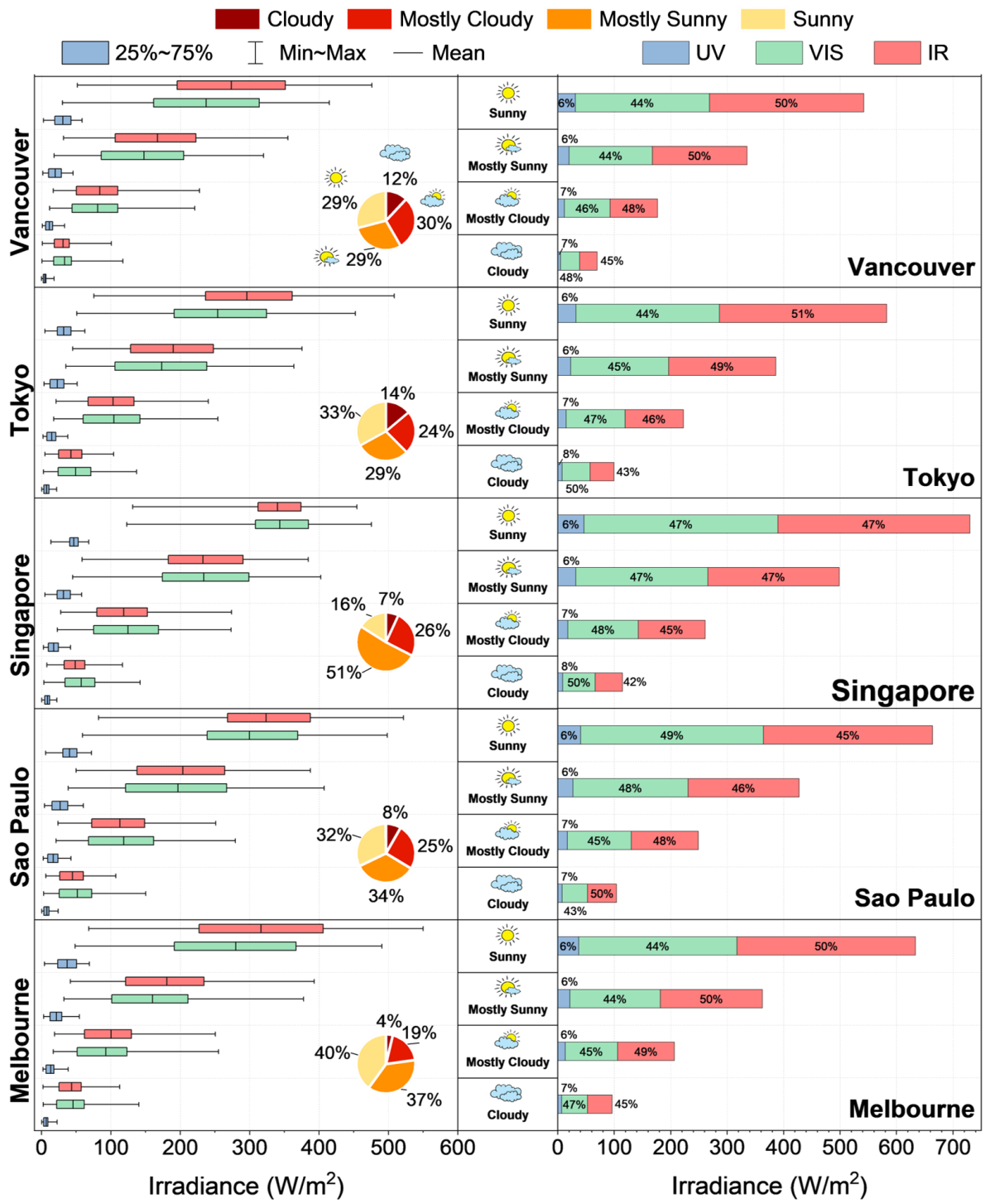


Fig. S2 Solar irradiance analysis of 5 selected cities under different cloud cover conditions. The results are based on a 10-year dataset (2013–2022). The left box plot showcases the irradiances of various wavelength ranges across varying cloudiness levels. The accompanying pie chart displays the distribution of cloud cover conditions during the analysed period. On the right, stacked bars represent the average total irradiances under different cloud cover conditions, while the percentage contribution of each wavelength region is visualized.

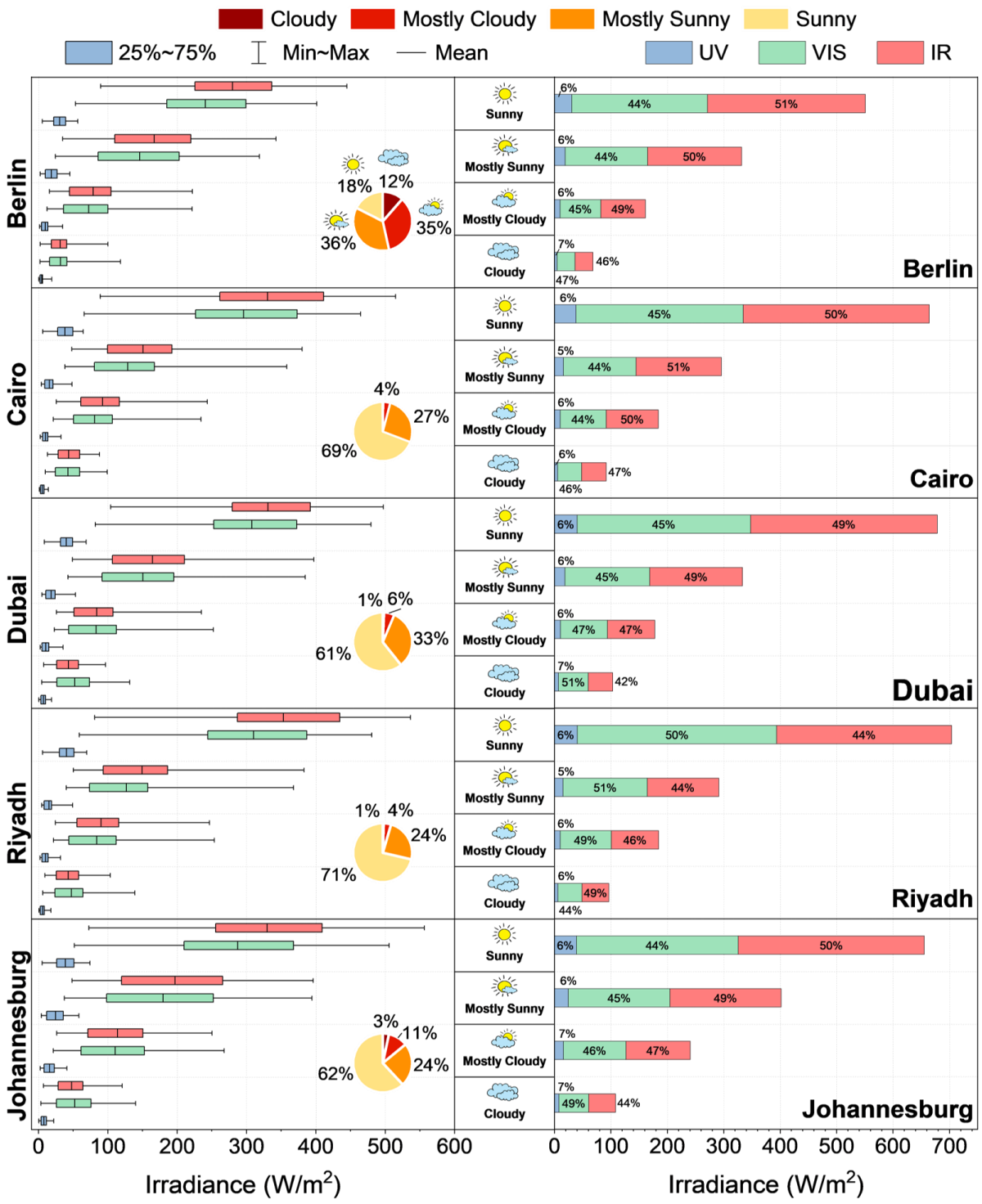


Fig. S3 Solar irradiance analysis of 5 selected cities under different cloud cover conditions. The results are based on a 10-year dataset (2013–2022). The left box plot showcases the irradiances of various wavelength ranges across varying cloudiness levels. The accompanying pie chart displays the distribution of cloud cover conditions during the analysed period. On the right, stacked bars represent the average total irradiances under different cloud cover conditions, while the percentage contribution of each wavelength region is visualized.

## References

1. M. A. Green, *Solar cells*, 1982, **7**, 337-340.